THE ASTROPHYSICAL JOURNAL, 514:287–295, 1999 March 20

DISK AND OUTFLOW IN CEPHEUS A–HW2: INTERFEROMETRIC SIO AND HCO^+ OBSERVATIONS

JOSÉ F. GÓMEZ
Laboratorio de Astrofísica Espacial y Física Fundamental, INTA, Apdo. Correos 50727, E-28080 Madrid, Spain
ANNEILA I. SARGENT
Division of Physics, Mathematics and Astronomy, 105-24, California Institute of Technology, Pasadena, CA 91125
JOSÉ M. TORRELLES
Instituto de Astrofísica de Andalucía, CSIC, Apdo. Correos 3004, E-18080 Granada, Spain; and Instituto Mediterráneo de Estudios Avanzados (CSIC-UIB), Universitat de les Illes Balears, E-07071 Palma de Mallorca, Spain
PAUL T. P. HO
Harvard-Smithsonian Center for Astrophysics, 60 Garden Street, Cambridge, MA 02138
LUIS F. RODRÍGUEZ AND JORGE CANTÓ
Instituto de Astronomía, Universidad Nacional Autónoma de México, Apdo. Postal 70-264, DF 04510, Mexico
AND
GUIDO GARAY
Departamento de Astronomía, Universidad de Chile, Casilla 36-D, Santiago, Chile
Received 1998 April 8; accepted 1998 October 29

ABSTRACT

This paper reports observations of the HCO^+ $(1 \rightarrow 0)$ and SiO $(2 \rightarrow 1)$ lines and of continuum emission at $\lambda = 3.4$ mm toward the Cepheus A East star-forming region. The HCO^+ line shows emission up to velocities of ~ 50 km s^{-1} relative to the ambient cloud velocity. The spatial distribution of the high-velocity gas is bipolar, centered on HW2, and extends for $\sim 1'$ along P.A. $= 55°$–$60°$. The orientation of this molecular outflow is very similar to that of the radio jet and CO emission associated with HW2. This confirms that current mass loss from HW2 takes place in the northeast-southwest direction. The momentum rate of the HCO^+ outflow is $1.3 \times 10^{-2}\ M_\odot$ km s^{-1} yr^{-1}, 20 times larger than that of the ionized jet from HW2, suggesting that the jet could be largely neutral. Peaks of HCO^+ emission coincide with some of the radio-continuum sources in the region, consistent with outflow–ambient gas interaction. Multiple episodes of outflow activity from either one precessing source or a number of powering sources would explain the detection of moderate-velocity HCO^+ emission toward the HW7 chain of sources. The continuum emission at 3.4 mm is strongly peaked toward HW2, confirming that this is the most likely powering source for the outflow. The SiO emission is barely elongated along P.A. $= -33°$, i.e., almost perpendicular to the HCO^+ outflow. A velocity trend consistent with a gradient of ~ 31 km s^{-1} over $2''$ is detected along the major axis of the SiO structure; these motions could be bound by $200\ M_\odot$. Published H_2O and CS observations support our suggestion that this represents the outer, ~ 750 AU radius, part of a circumstellar disk, although further observations are needed to confirm this interpretation.

Subject headings: ISM: individual (Cepheus A) — ISM: jets and outflows — ISM: molecules — stars: pre–main-sequence

1. INTRODUCTION

The Cepheus A region is extremely rich in observational phenomena related to star formation (Torrelles et al. 1993), making it especially well suited to studies of the relationship between these phenomena, and in particular the connection between small-scale jets, interstellar molecular outflows, and dense gas. At a distance of 725 pc (Johnson 1957), Cepheus A was identified as the densest component within the molecular cloud complex associated with Cepheus OB3 (Sargent 1977, 1979), and includes one of the first bipolar molecular outflows reported (Rodríguez, Ho, & Moran 1980). On scales of ~ 1 pc, the outflow follows a bipolar distribution, roughly in the east-west direction (Rodríguez et al. 1980; Ho, Moran, & Rodríguez 1982), but at $\sim 15''$ resolution ($\sim 0''.05$ pc) the morphology appears more complex, and even quadrupolar (Hayashi, Hasegawa, & Kaifu 1988; Bally & Lane 1991). Based on observations of the high-velocity outflow and the high-density gas traced by NH_3, Torrelles et al. (1993) proposed that the originally bipolar outflow could have been split and redirected by the dense gas, giving rise to the observed quadrupolar morphology. More recently, Narayanan & Walker (1996, hereafter NW96), employing molecular line observations at resolutions ranging from $10''$ to $20''$, have suggested that the morphology may reflect multiple outflow episodes. They postulate that the older (3–20×10^4 yr) high-velocity outflow is oriented along the east-west direction, while the extremely high velocity lobes of the current ($\leq 5 \times 10^3$ yr) flow extend to the northeast and southwest.

Sixteen radio-continuum sources have been detected in Cepheus A East (Hughes & Wouterloot 1984 [HW]; Garay et al. 1996). Of these, at least two, HW2 and HW3d, show signs of harboring internal excitation sources (Torrelles et al. 1986; Garay et al. 1996), undergoing mass loss. The most likely powering source for the molecular outflow is HW2. The radio-continuum emission from this source is elongated, with a deconvolved size of $\sim 0''.8 \times 0''.1$ (580×73 AU, P.A. $= 48°$) at 3.6 cm (Rodríguez et al. 1994). At shorter wavelengths, it is resolved into two emission peaks separated by $\sim 0''.1$ (Hughes 1988; Torrelles et al. 1996). The spec-

tral index of the radio-continuum emission and the dependence of its size with frequency were interpreted by Rodríguez et al. (1994) as being consistent with emission from a biconical ionized thermal jet (cf. Reynolds 1986). Further support for this interpretation comes from a recent study of the dependence with frequency of the separation of the two emission peaks (Torrelles et al. 1996). Perpendicular to the jet, 28 maser spots extend along P.A. $= -48°$; their velocity field is consistent with a disk of ~ 300 AU radius simultaneously undergoing rotation and contraction (Torrelles et al. 1996). The CS measurements of NW96 also indicate the presence of a rotating structure centered on HW2 at P.A. $= -45°$, but with radius of 0.16 pc.

The analysis of NW96 presents a plausible geometry for the Cepheus A East region. Nevertheless, a more detailed understanding of the relationship between the parsec-scale molecular outflow, the 600 AU biconical radio jet, and the putative disk requires molecular line observations on smaller scales. The observations presented in this paper, at angular resolution $\sim 3''$ (~ 0.01 pc), provide a link between these different scales.

2. OBSERVATIONS AND DATA REDUCTION

Observations of the HCO^+ $(1 \rightarrow 0)$ (rest frequency $v = 89.188518$ GHz) and SiO $(2 \rightarrow 1, v = 0)$ (rest frequency $v = 86.846998$ GHz) lines were made with the Owens Valley Radio Observatory (OVRO) millimeter-wave array between 1993 November and 1994 February. Three configurations of five 10.4 m telescopes with baselines ranging from 15 to 206 m resulted in synthesized beams of $3''.2 \times 2''.6$ (FWHM) at P.A. $= -80°$ (uniform weighting) and $4''.7 \times 3''.7$ (FWHM) at P.A. $= -85°$ (natural weighting). The phase center was located at $\alpha(1950) = 22^h54^m19^s.00$, $\delta(1950) = 61°45'47''.3$.

The double-sideband mode enabled us to observe both lines at the same time, with HCO^+ in the upper sideband and SiO in the lower. Cryogenically cooled SIS receivers on each telescope provided typical SSB system temperatures of 300–400 K, corrected for antenna and atmospheric losses and for atmospheric incoherence. For each line, the digital correlator was configured to have two bands of Hanning-smoothed channels, one 32 MHz and the other 8 MHz wide. Each comprised 64 channels, leading to spectral resolutions of 0.5 MHz (1.7 km s^{-1}) and 0.125 MHz (0.4 km s^{-1}), respectively. All bands were centered at $V_{LSR} = -11.16$ km s^{-1}. Simultaneous continuum measurements were made using an analog correlator of bandwidth 1 GHz (which included both continuum and line emission).

The quasars 0016+731, 0528+134, and 2037+511 were observed at intervals of about 20 minutes to track gain and phase variations. Measurements of Uranus and Neptune, as well as 3C 273, 3C 345, and 3C 454.3, provided the absolute flux density scale. Resulting uncertainties are $\sim 20\%$. Initial calibration was carried out using the Caltech MMA data reduction package (Scoville et al. 1993).

Further data processing employed the Astronomical Image Processing System (AIPS) of the National Radio Astronomy Observatory. The 1 GHz bandwidth continuum visibilities were self-calibrated. The phase and intensity corrections thus obtained were then applied to their respective line visibilities. Two sets of pure continuum data were constructed by averaging the visibilities of line-free channels. This continuum emission was subtracted from the line data using the task UVSUB of AIPS. The final maps presented in this paper were obtained with uniform (HCO^+ data) and natural (SiO data) weighting of the visibilities. Positional uncertainties are of the order of $0''.5$.

3. RESULTS

3.1. HCO^+

The $HCO^+(1 \rightarrow 0)$ spectra display strong self-absorption at velocities close to that of the ambient cloud, -11.15 km s^{-1}. Outside this velocity range, however, significant emission is detected. Figure 1 shows a map of the velocity-integrated HCO^+ emission for $|v - v_0| \gtrsim 10$ km s^{-1}, where v_0 is the ambient cloud velocity, superimposed on the NH_3 map of Torrelles et al. (1993). The high-velocity emission is clearly bipolar, and appears to be centered on the continuum source HW2 (represented by a filled circle). Blueshifted emission lies to the northeast and redshifted emission to the southwest. The total extent of the outflow is $\sim 1'$ (0.2 pc), along P.A. $\simeq 55°$–$60°$.

Outflow properties are further illustrated by Figure 2, where maps of the high-velocity HCO^+ emission in different velocity ranges are presented. As expected from Figure 1, blueshifted emission lies predominantly to the northeast of HW2, while the redshifted emission is in the southwest. At higher velocities, the emitting gas is observed increasingly farther from the center of the outflow.

Typical spectra for each area are shown in Figures 3 and 4. In the northeast spectrum, at $(17''.0, 13''.0)$ offset from the phase center, emission is detected up to velocities of $V_{LSR} \simeq -47$ km s^{-1} with respect to the ambient cloud; in the southwest, at $(-15''.5, -12''.0)$ from the phase center, emission is seen up to velocities of $\gtrsim 39$ km s^{-1}. Since the high-velocity emission in the southwest approaches the edge of the spectral band, it may extend to even higher velocities. HCO^+ spectra toward HW2, at the two different spectral resolutions (Fig. 4), show limited wing emission and strong self-absorption.

Physical parameters for each lobe of the HCO^+ outflow are summarized in Table 1. This table gives, for each lobe, the velocity range of the line wings, the maximum line intensity integrated over this range, the maximum column density of the outflowing gas, the flux density integrated over the given velocity range, the total mass, the momentum rate, and the mechanical luminosity of the outflow. In calculating these parameters, we assume LTE and optically thin emission in the line wings. We also adopt an excitation temperature $T_{ex} = 25$ K (the temperature assumed for the CO emission by NW96), a dipole moment for the HCO^+ molecule of $\mu = 3.3$ D, and an abundance of HCO^+ relative to H_2, X_{HCO^+}, of 10^{-8}.

3.2. SiO

The SiO emission detected is closely associated with source HW2, its peak position being coincident with the position of the continuum radio source, although some low-level emission could be associated with other continuum sources in the region (Fig. 5). Figure 4 (*bottom panels*) shows the SiO spectrum at the position of the HW2 object, observed with velocity resolutions of 1.68 km s^{-1} (*left*) and 0.42 km s^{-1} (*right*). A map of the SiO emission integrated over the velocity range -33.6 to 14.8 km s^{-1} is shown in Figure 6*a*. The source appears to be barely resolved, and is centered on the position of the continuum radio source HW2. Although the deconvolved size [$\simeq 4''.7(\pm 0''.2) \times$

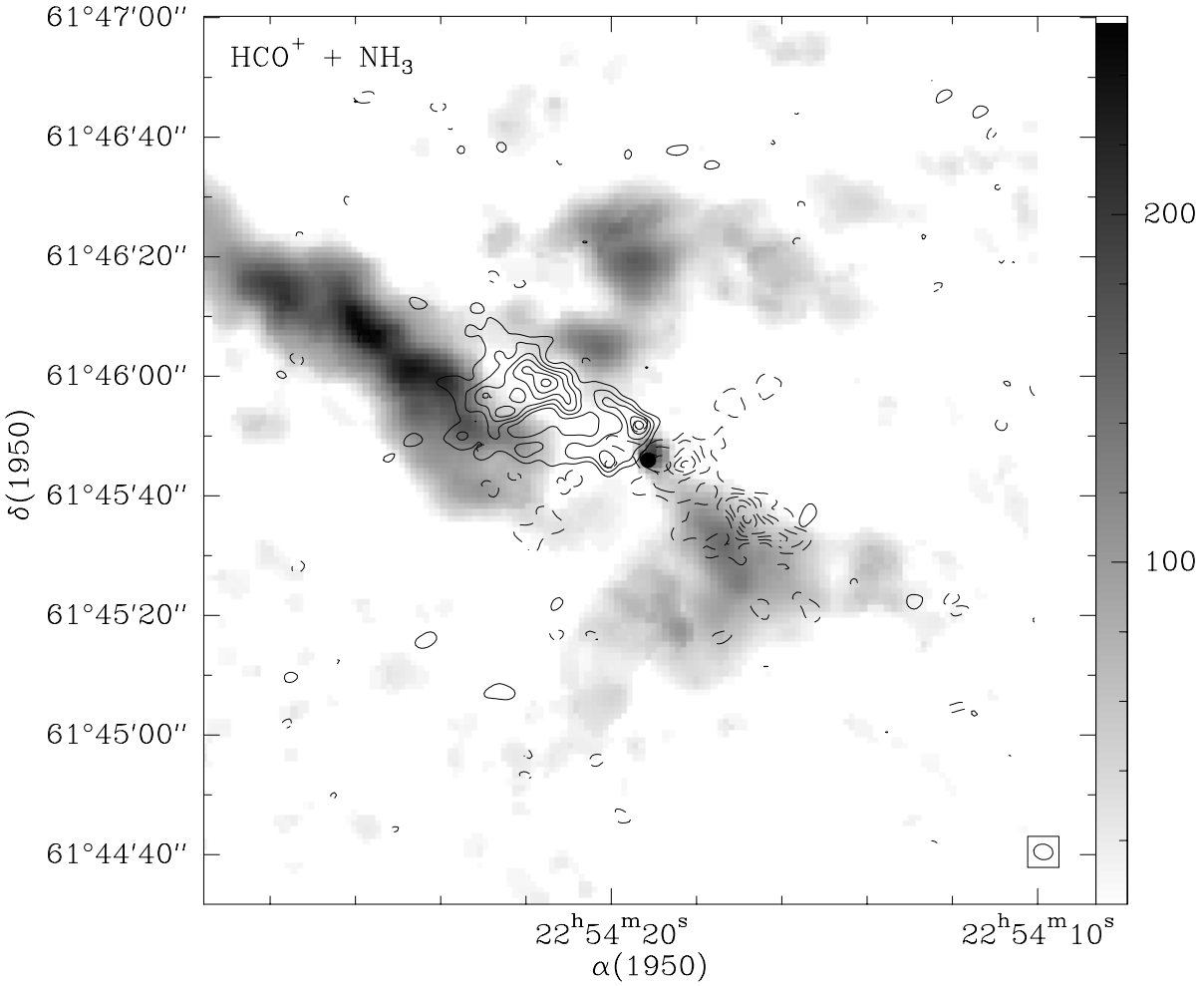

FIG. 1.—Integrated intensity map of $HCO^+(J = 1 \rightarrow 0)$ emission over the velocity ranges -61.5 to -21.3 km s^{-1} (*solid contours*), and -1.1 to 39.2 km s^{-1} (*dashed contours*) superimposed on the NH_3 emission (Torrelles et al. 1993). The lowest contour and the increment step are 504 mJy beam^{-1} km s^{-1} (3 σ). The filled circle marks the position of the continuum source HW2.

3.″6(±0.″2), FWHM] is comparable to our beam size (≃4.″7 × 3.″7), the orientations (P.A. = −33° and −85°, respectively) are such that we suggest a small degree of SiO elongation almost perpendicular to the high-velocity HCO^+ outflow axis (P.A. = 55°–60°). The position of the emission peak shifts slightly with velocity around HW2 (see Fig. 5). A position-velocity diagram along the major axis of the SiO structure (Fig. 7*a*) shows a trend that is consistent with a velocity gradient of ∼31 km s^{-1} along ∼2″ (1500 AU). No such gradient is seen along the minor axis of the SiO structure (Fig. 7*b*), which would correspond to the HCO^+ outflow direction. We estimate that a mass of ∼200 $M_\odot$ would be necessary to gravitationally bind the observed motions along the major axis of the SiO structure. This is somewhat smaller than the value of 330 $M_\odot$ derived by NW96 for the rotating CS structure of 0.32 pc diameter.

A comparison of our SiO results with single-dish observations (Martín-Pintado, Bachiller, & Fuente 1992) indicates that most of the SiO emission around HW2 derives from the compact structure. We observe an integrated flux density of 8.53 ± 0.04 Jy km s^{-1}, while these authors obtained ∼7 Jy km s^{-1} (1.7 K km s^{-1} over a 26″ beam). Evidently, the interferometer is not missing a significant amount of flux as a result of the lack of short spacings.

3.3. *Continuum*

Figure 6*b* shows a map of continuum emission obtained by averaging line-free channels from both HCO^+ and SiO spectral data. Because of their slightly different frequencies, these data sets have different angular resolutions, even using the same visibility weightings. They were therefore convolved with a Gaussian beam of 3.″5 before the final averaging. The continuum emission is strongly peaked at the position of HW2, with a maximum intensity of 179 ± 3 mJy and a total flux density of 315 ± 15 mJy. Although HW2, the HW3 group, HW4, HW8, and HW9 may all contribute to the observed total flux density, Figure 6*b* demonstrates that the continuum emission is dominated by HW2. Our data do not have sufficient angular resolution to study the morphology of the continuum emission associated with each of the HW sources in detail. Some elongation toward the northeast is evident in the lowest levels of the continuum emission (Fig. 6*b*). This orientation is similar to that of the HCO^+ outflow, although this morphology could be the effect of the integration of the different continuum sources in the region.

Our 3.″5 beam is large enough to include all the emission from HW2 (which is ∼0.″8 in size at 3.6 cm), so that at least

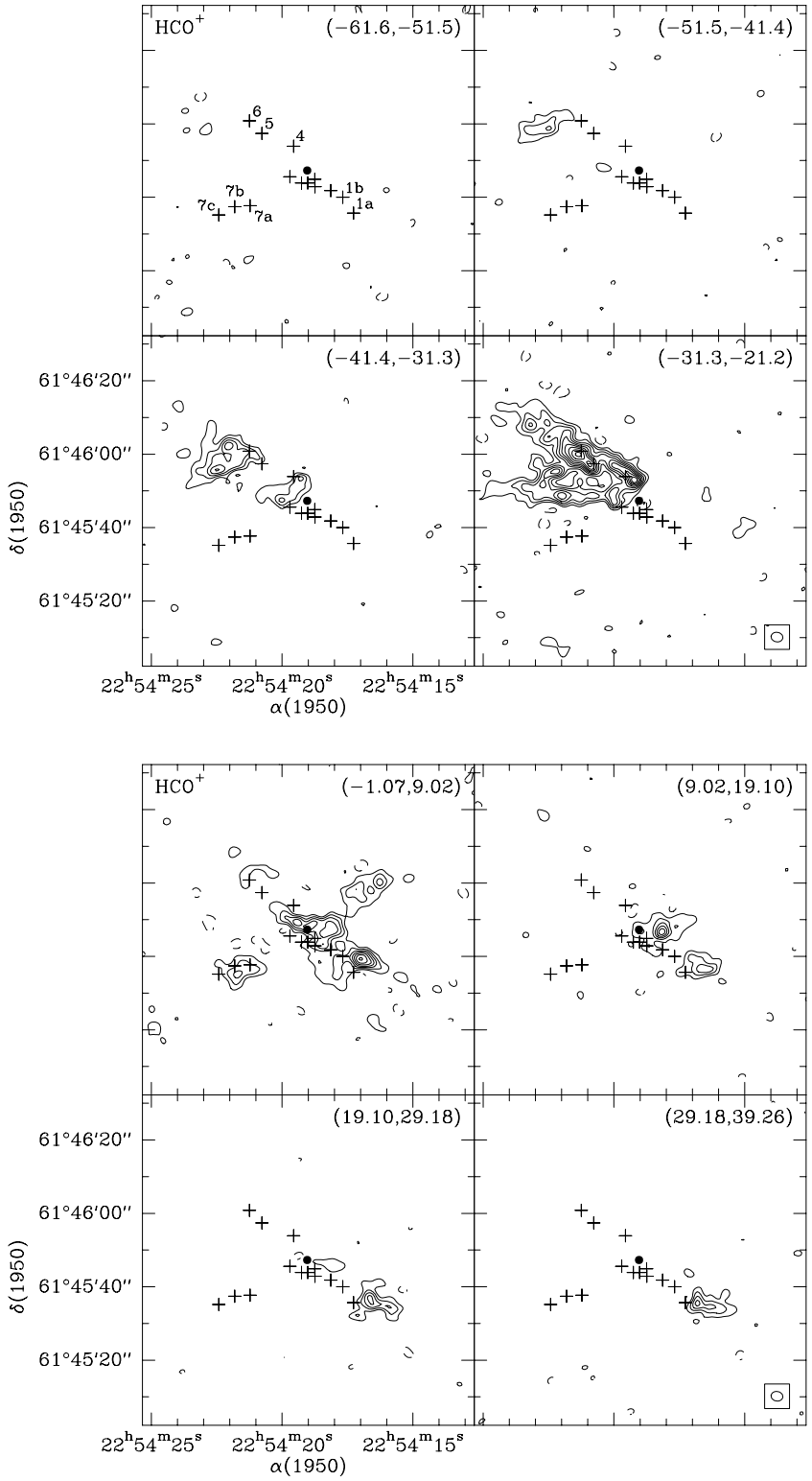

FIG. 2.—Integrated intensity maps of $HCO^+(J = 1 \rightarrow 0)$ blue- and redshifted emission, over different velocity ranges. The velocity range is indicated at the top right corner of each panel. The lowest contour level and the increment step are 227 mJy beam^{-1} km s^{-1} (3 times the rms of the map). The size of the synthesized beam is $3''.2 \times 2''.6$, P.A. $= -80°$; the beam is shown at the bottom right corner of the figure. Crosses mark the position of the centimeter radio-continuum sources (Garay et al. 1996). The filled circle indicates the position of HW2. Some of these radio-continuum sources are labeled with their HW numbers (see Fig. 6 for identification of the central sources).

179 mJy must be attributed to this source. For the ionized jet, the expected flux at 3.4 mm calculated on the basis of an $S_\nu \propto \nu^{0.69}$ power law (Rodríguez et al. 1994) would be only 55 mJy. However, the exact contribution of the jet to this 3.4 mm continuum emission is difficult to estimate, since, for instance, the flux density from HW2 at 1.3 cm measured by Torrelles et al. (1996) 4 yr later than the Rodríguez et al. (1994) observations is a factor of 2 higher than expected

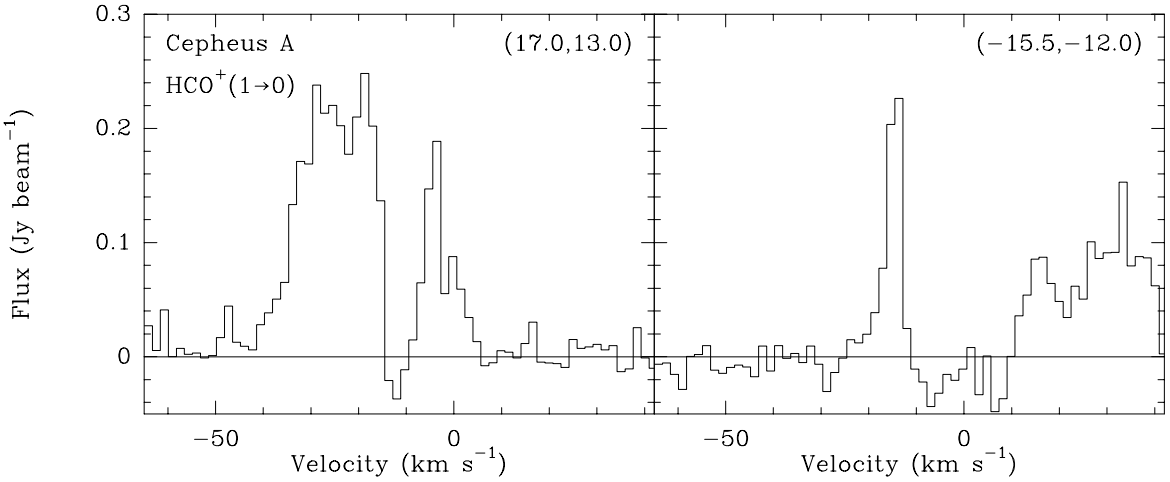

FIG. 3.—Spectra of the HCO^+ ($J = 1 \rightarrow 0$) transition at selected positions, to the northeast (*right*) and southwest (*left*) of HW2. Position offsets, in arcseconds, from the phase center are shown in the top right corner of each spectrum.

from the power law, suggesting that the emission from HW2 is variable.

4. DISCUSSION

4.1. *The Molecular Outflow*

NW96 have proposed a model that explains the various observations of Cepheus A in terms of at least two outflows interacting with a clumpy ambient cloud. The older flow is larger and oriented east-west, while the most recent is oriented northeast-southwest. Our observations allow us to make a more detailed comparison of the model and the available observations.

Our new maps (Figs. 1 and 2) clearly show that at scales of $\lesssim 0.1$ pc, the molecular outflow is bipolar and highly collimated along an axis at P.A. = 55°–60°. The total extent of the outflow is $\sim 1'$. These maps nicely complement the lower resolution CO results of NW96, which indicated the presence of a relatively young, extremely high-velocity outflow along P.A. = 40°–60°. It is clear from Figures 1 and 2 that lower velocity material also contributes to this outflow. Strong emission is evident at $|v - v_0| < 10$ km

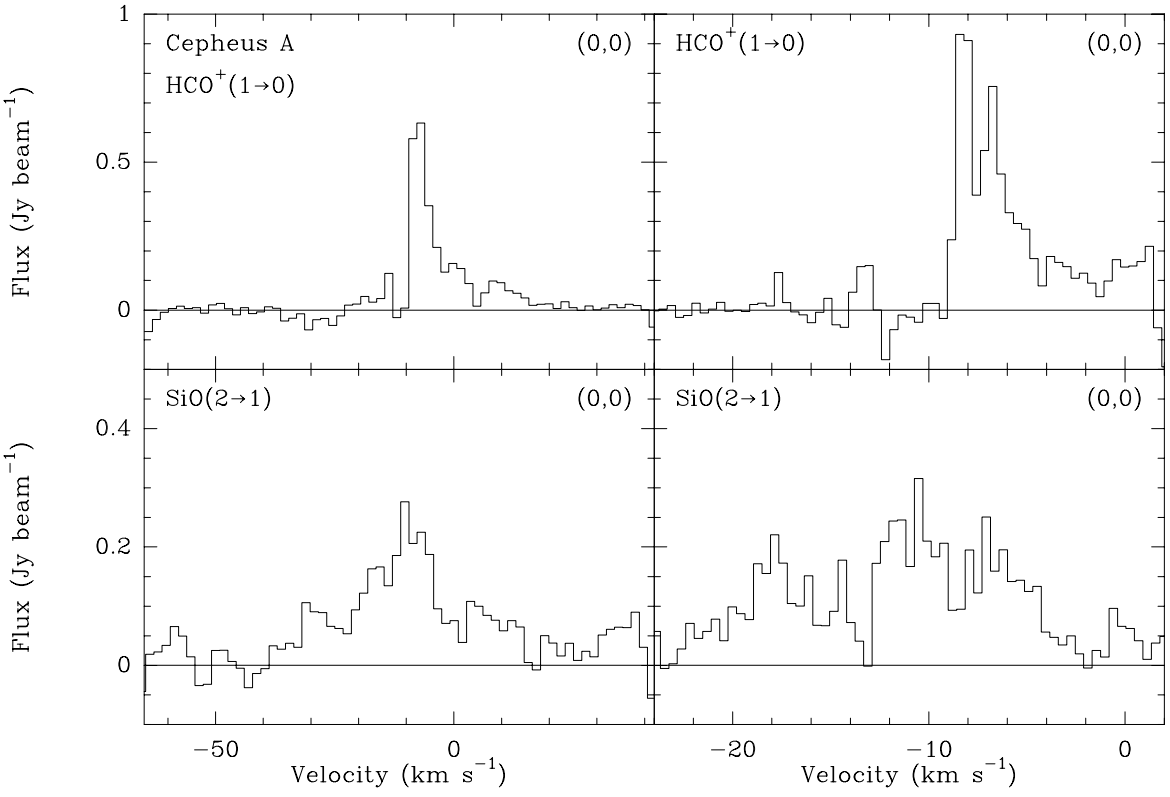

FIG. 4.—Spectrum of the HCO^+ ($J = 1 \rightarrow 0$) (*top*) and SiO ($J = 2 \rightarrow 1$) (*bottom*) transitions at the position of source HW2, with two different velocity resolutions (*left*, $\Delta V = 1.7$ km s^{-1}; *right*, $\Delta V = 0.4$ km s^{-1}).

TABLE 1

PHYSICAL PARAMETERS OF THE OUTFLOW

Parameter	Red Lobe	Blue Lobe
V_{LSR} (km s^{-1})	(0.2, 38.4)	(−47.3, −22.1)
$\int I\,dV$ (Jy beam^{-1} km s^{-1})	3.2	3.2
$N(H_2)$ (10^{22} cm^{-2})[a]	1.5	1.5
$\iint I\,dV\,d\Omega$ (Jy km s^{-1})[b]	37.1	60.0
M ($M_\odot$)[c]	0.33	0.53
R (cm)[d]	3.3×10^{17}	4.6×10^{17}
$\dot{P}$ ($M_\odot$ km s^{-1} yr^{-1})[e]	7.9×10^{-3}	4.8×10^{-3}
L_{mec} ($L_\odot$)[f]	32	14

[a] Maximum column density of the outflow, calculated from $N = 3.958 \times 10^{14}\, X^{-1}(\theta_a \times \theta_b)^{-1} \int I\,dV$, where X is the abundance of HCO^+ with respect to hydrogen (assumed to be 10^{-8}), and θ_a and θ_b are the FWHM sizes (in arcseconds) of the major and minor axes of the beam, respectively.

[b] Line intensity, integrated over the mentioned velocity range and over the spatial extent of the lobe.

[c] Mass of the outflow, obtained from $1.680 \times 10^{-16}\, D^2 X^{-1} \iint I\,dV\,d\Omega$, where D is the distance to the source (in parsecs).

[d] Maximum distance from the central source to the high-velocity emission.

[e] Momentum rate, $\dot{P} \simeq MV^2_{max}/R$, where V_{max} is the maximum velocity observed in the wing with respect to the line center (−11.15 km s^{-1}).

[f] Mechanical luminosity, $L_{mec} \simeq MV^3_{max}/2R$.

s^{-1}. As expected, the lower velocity gas is located closer to the central star (Shu et al. 1991). The position of HW2 at the center of the HCO^+ outflow and the strongly peaked 3.4 mm continuum emission toward this source confirms that it is the most likely powering source for the outflow. The lobe geometry appears to be consistent with the x-wind model, which predicts a wider outflow close to the star (see, e.g., Li & Shu 1996). The bases of the lobes subtend $\sim 130°$ from HW2, which requires the presence of a low-collimation wind, despite the narrow opening angle of the jet ($\sim 23°$; Torrelles et al. 1996), while farther from the central star the outflow becomes more collimated ($\lesssim 30°$ for the highest velocity components). The x-wind model suggests that highly collimated jets are "optical illusions," since their emission is dominated by the central, denser areas, but there exist lower collimation winds that can power molecular outflows with wide opening angles close to the star (Shu el al. 1995; Shang, Shu, & Glassgold 1998). We do note that the x-wind models were constructed for low-mass stars. Their application to high-mass stars is uncertain.

One remarkable result shown in Figure 2 is the excellent alignment of the HCO^+ outflow and the radio-continuum sources HW1, HW2, HW4, HW5, and HW6. The alignment was indicated by the measurements of NW96, but it is much more obvious here. In particular, the peaks of the high-velocity blueshifted HCO^+ emission appear to coincide with the positions of some of the continuum sources (Fig. 2). The northeast-southwest orientation of the HCO^+ outflow and the radio-continuum sources agrees well with that of the bipolar, partially ionized HW2 jet at P.A. = 44°–48° (Rodríguez et al. 1994; Torrelles et al. 1996). Together with the high-velocity CO (NW96) and H_2 images (Doyon & Nadeau 1988; Lane 1989; Hartigan et al. 1996), and the presence of the HH-NE object (Corcoran, Ray, & Mundt 1993), these data show unambiguously that considerable mass outflow takes place in this direction on scales of up to ~ 0.4 pc. The east-west–oriented, parsec-scale outflow that gives rise to the quadrupolar outflow structure noted by Bally & Lane (1991) was not detected in our maps. This is undoubtedly due to our small primary beam and to the fact that the interferometer is insensitive to structures larger than 60″. In fact, an east-west HCO^+ outflow, similar in size scale to the CO flow of NW96, was seen in early HCO^+ single-dish observations by Loren et al. (1984).

In Figure 2, the location of the maxima of the blueshifted HCO^+ emission, close to radio-continuum sources and along the edges of the high-density structure Cep A–3 traced by NH_3 (Torrelles et al. 1993), is certainly suggestive of an interaction between the outflow and the ambient medium. These radio-continuum sources could trace shock-ionized gas (Torrelles et al. 1986; Garay et al. 1996), while the molecular peaks reflect increased collisional excitation of the HCO^+ molecule by electrons (Wolfire & Königl 1993). Torrelles et al. (1993) noted enhanced NH_3 rotational temperatures close to the continuum sources, consistent with this interpretation. In addition, the CO extremely high velocity blue lobe bends near the Cep A–3 NH_3 clump, as if being redirected (NW96). It has been suggested that the dense NH_3 structures Cep A–1 and Cep A–3 (Torrelles et al. 1993) are part of the outflow (e.g., Staude & Elsässer 1993). This seems unlikely, since most of the HCO^+ high-velocity emission we detect here (Fig. 1) lies between the dense structures.

The intermediate-velocity HCO^+ emission found around the chain of sources HW7a, b, and c does not fit easily into the scheme of a single stationary powering source for the outflow. If the high-velocity gas near the HW7 chain is also due to a wind from HW2, then part of this wind must be ejected almost perpendicular to the current dominant wind direction, which does not seem very likely. However, this can be resolved if during its evolution HW2 has undergone multiple episodes of outflow activity ("outbursts") with different orientations (e.g., precessing source), as suggested by NW96. Alternatively, although it seems clear that HW2 is the dominant powering source in the region, another source might also be undergoing mass loss. For instance, Garay et al. (1996) suggested that the source HW3d (which seems to have an internal excitation source) is also ionizing the gas and producing the chain of radio sources HW7.

The total momentum rate and mechanical luminosity of the outflow ($1.3 \times 10^{-2}\ M_\odot$ km s^{-1} yr^{-1} and 46 $L_\odot$, respectively; see Table 1) are consistent with the values found by Ho et al. (1982) and NW96. However, this momentum rate is at least 20 times larger than that of the ionized component of the jet ($6 \times 10^{-4}\ M_\odot$ km s^{-1} yr^{-1}), indicating that the jet is largely neutral, if it drives the current outflow. The momentum rate of the outflow and the centimeter continuum luminosity of HW2, its powering source ($S_{3.6\,cm} d^2 = 5.15$ mJy kpc^2, from Rodríguez et al. 1994 data), are close to the correlation given by Anglada (1996) for these two parameters in outflow sources [$\dot{P} = 10^{-2.5}(S_\nu d^2)^{1.1}$]. Of course, this statistical correlation was derived for low-mass sources, and further studies will be necessary to confirm the correlation for other high-mass stars.

4.2. *The Circumstellar Disk*

Torrelles et al. (1996), taking into account the HCO^+ data presented in this paper, suggested that the kinematical and spatial distribution of the water masers around HW2

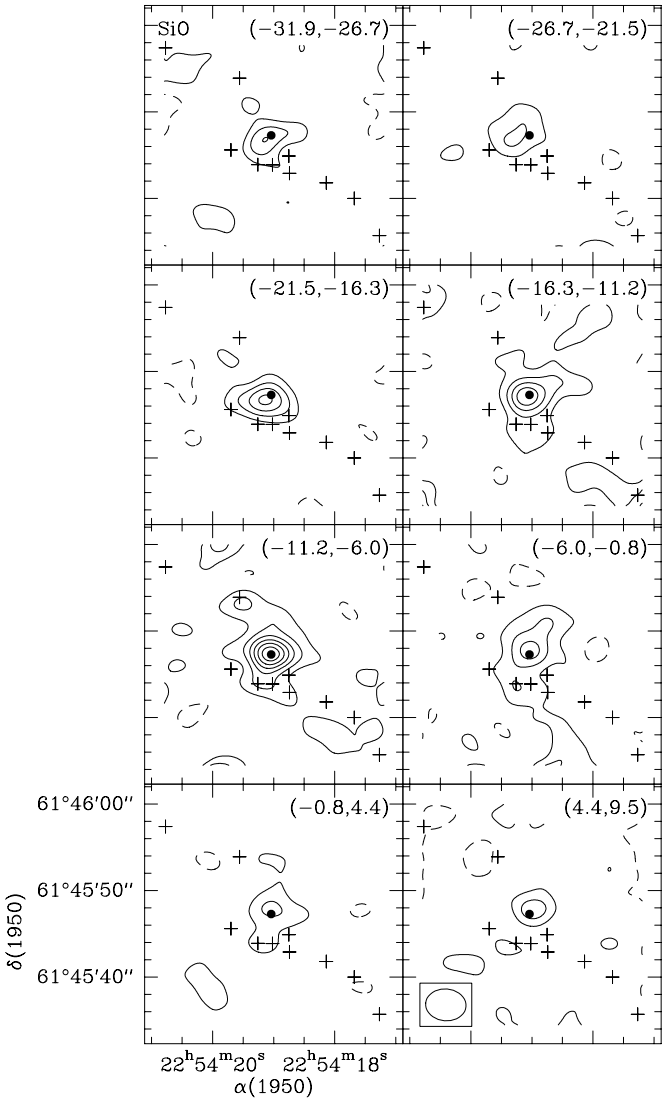

FIG. 5.—Integrated intensity maps of SiO ($J = 2 \rightarrow 1$) over different velocity ranges. The velocity range is indicated at the top right corner of each panel. The lowest contour level and the increment step are 180 mJy beam^{-1} km s^{-1} (3 times the rms of the map). The size of the synthesized beam is 4″.7 × 3″.7, P.A. = −85°. Symbols have the same meaning as in Fig. 2.

could be tracing a disk of 300 AU radius undergoing rotation and contraction. This proposed disk has its major axis along P.A. = −48°, nearly perpendicular to the radio jet and to the HCO^+ molecular outflow.

Our SiO observations are compatible with the presence of this disk structure. Although the elongation of the SiO integrated emission is marginal, we think that it is significant when combined with other observational evidence. Its orientation (P.A. = −33°) is close to that of the H_2O maser distribution (P.A. = −48°) and the CS velocity gradient (P.A. = −45°; NW96). All lie at essentially right angles to the radio jet and the HCO^+ bipolar outflow, as expected. In addition, the velocity gradient of the SiO emission along its major axis (Fig. 7*a*) is of the same sign as that of the H_2O masers (see Fig. 2 of Torrelles et al. 1996) and the CS lines. Thus, the three molecules (H_2O, SiO, and CS) appear to trace a similar structure, although on different scales.

The SiO emission traces a gradient of ∼31 km s^{-1} over a scale of 1500 AU (that could be bound by 200 $M_\odot$), while the gradient seen with the masers is 30 km s^{-1} over 600 AU (bound by 70 $M_\odot$). NW96 estimate a mass of 330 $M_\odot$ for the CS core on the scale of 0.16 pc radius. We suggest that the SiO emission traces the outer part of a molecular circumstellar disk, of ∼750 AU radius, while the inner disk (∼300 AU radius) is traced by the H_2O masers, both structures being embedded in the CS core. No evidence of the contraction suggested by Torrelles et al. (1996) is observed in the SiO data (Fig. 7*b*) at the scales sampled here. If we assume a flat structure of 750 AU radius and 75 AU height for the SiO structure, a mean density of $\sim 2.5 \times 10^{11}$ cm^{-3} is required to account for 200 $M_\odot$. This density may be reasonable for circumstellar disks (e.g., Morfill, Tscharnuter, & Völk 1985). Molecular species can remain in the gas phase at this high density (Aikawa et al. 1997), despite their tendency to stick to dust grains in short timescales (see, e.g., van Dishoeck et al. 1993). Moreover, H_2O masers, such as those observed in this region, could survive such high densities without being thermalized (Strelnitskij 1984; Kylafis & Norman 1986). Given its radius of 750 AU, the SiO disk structure cannot be the agent directly responsible for the collimation of the thermal jet (whose minor axis is ∼73 AU). This collimation may be produced by the innermost

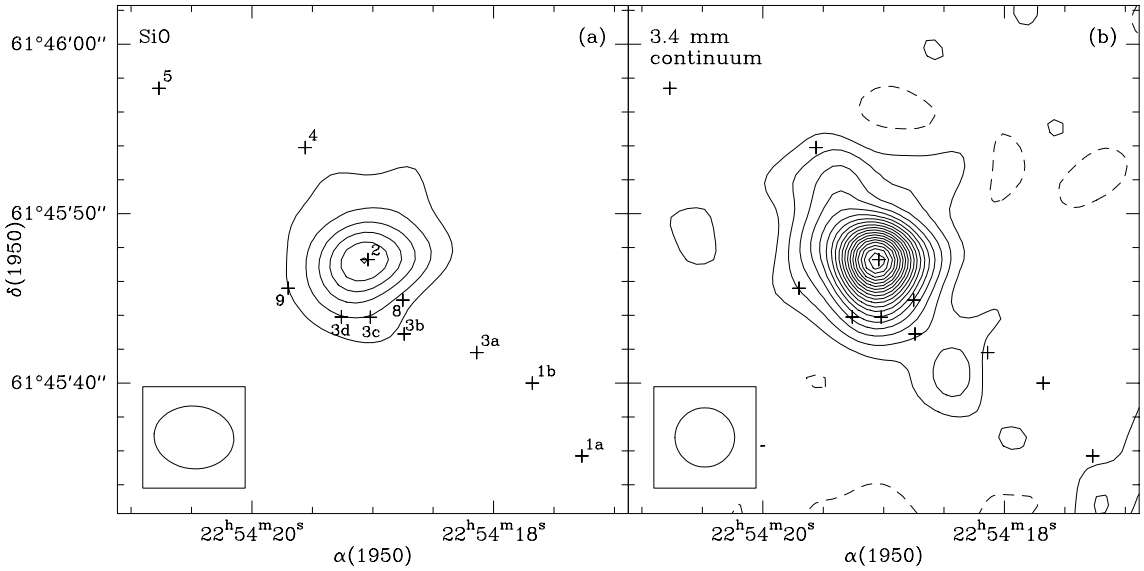

FIG. 6.—(*a*) Integrated intensity map of SiO ($J = 2 \rightarrow 1$) emission, over the velocity range -33.6 to 14.8 km s^{-1}. The lowest contour level and the increment step are 778 mJy beam^{-1} km s^{-1} (3 σ). The size of the synthesized beam is 4″.7 × 3″.7, P.A. = $-85°$. (*b*) Contour map of the continuum emission at 3.4 mm, obtained from line-free channels. The lowest contour level and the increment step are 9 mJy beam^{-1} (3 σ). The map has been convolved with a Gaussian to give a final resolution of 3″.5. Crosses in (*a*) and (*b*) mark the position of the centimeter radio-continuum sources (Garay et al. 1996), which are labeled with their HW numbers.

part of the proposed disk, or by a separate, more compact structure.

Our suggestion that the SiO emission is tracing a circumstellar disk needs further observational support. Direct evidence of the presence of a circumstellar disk will probably require molecular line observations with subarcsecond resolution (see, e.g., Gómez & D'Alessio 1995).

5. CONCLUSIONS

We have made interferometric HCO^+ ($1 \rightarrow 0$) and SiO ($2 \rightarrow 1$) observations using the Owens Valley Radio Observatory interferometer toward the star-forming region Cepheus A East. These observations allow us to study both the molecular outflow and the circumstellar molecular disk associated with source HW2.

The continuum emission at these wavelengths (3.4 mm) is strongly peaked toward HW2, which confirms this as the most likely powering source of the molecular outflow. The 3.4 mm flux associated with this source is about a factor of 3 larger than the extrapolation of the biconical jet model presented by Rodríguez et al. (1994) and Torrelles et al. (1996). However, the exact contribution of the jet to the total continuum emission is uncertain, given the variability of the jet emission at centimeter wavelengths.

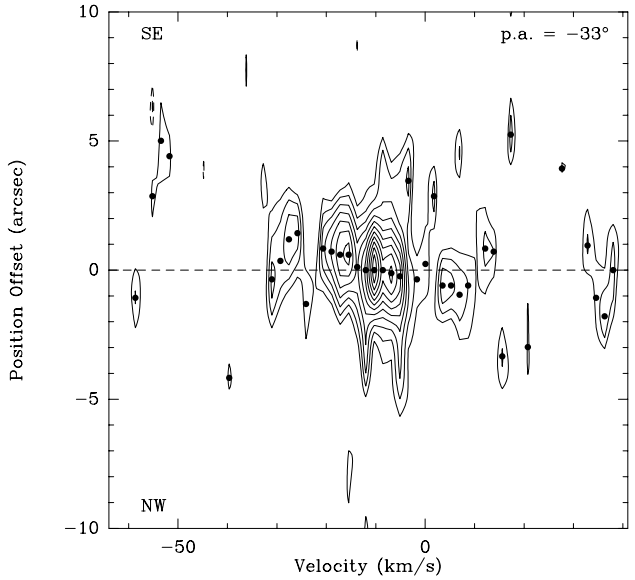

FIG. 7*a*

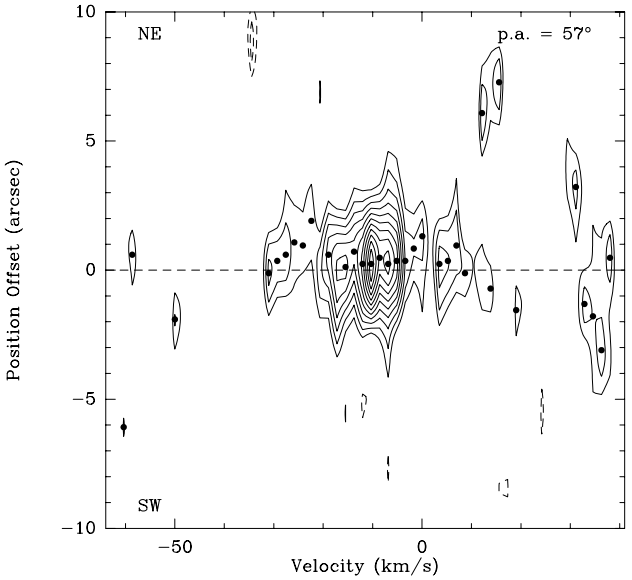

FIG. 7*b*

FIG. 7.—Position-velocity diagrams of the SiO emission, along directions with (*a*) P.A. = $-33°$ and (*b*) P.A. = 57°. The lowest contour level is 60 mJy beam^{-1} and the increment step is 20 mJy beam^{-1} (1 σ). The position offsets are relative to the phase center of the observations (the position of HW2). Position offsets are positive toward northern positions. Filled circles indicate the location of the intensity peaks at each velocity channel.

We find HCO^+ emission up to velocities of $\gtrsim 50$ km s^{-1} relative to the ambient cloud velocity. The spatial distribution of the high-velocity gas is bipolar, centered on HW2, and extends for $\sim 1'$ along P.A. $= 55°$–$60°$. This orientation is very similar to that of the ionized jet and CO emission associated with HW2, and confirms that the mass-loss phenomena from HW2 take place along the northeast-southwest direction. Peaks of HCO^+ emission coincide with some of the radio-continuum sources in the region, consistent with interaction between the outflow and the ambient molecular gas.

The SiO emission is relatively compact (FWHM size of $\simeq 4\farcs5 \times 3\farcs5$), and shows a small degree of elongation, with its major axis oriented with P.A. $= -33°$, almost perpendicular to the molecular outflow. A velocity gradient of ~ 31 km s^{-1} along $2''$ (1500 AU) is detected along the major axis of the SiO structure, which can be explained as gravitationally bound motions around $\sim 200\ M_\odot$. This gradient, and the similarity to the H_2O maser and CS distributions, support our suggestion that this represent the outer part of a circumstellar disk of ~ 750 AU radius, with the H_2O maser disk lying within it. Further observations are needed to confirm this interpretation.

We thank Paola Caselli for discussions on SiO chemistry. Research at the Owens Valley Radio Observatory is supported by the National Science Foundation through NSF grant AST 96-13717. J. F. G. and J. M. T. are supported in part by DGICYT grant PB95-0066 and by Junta de Andalucía (Spain). J. F. G. is also supported by INTA grant IGE 4900506. L. F. R. acknowledges the support of DGAPA, UNAM, and CONACyT (Mexico). G. G. acknowledges support from the Chilean Fondecyt project 1980660. J. F. G. also thanks CalTech for their hospitality during part of the data reduction. J. M. T. acknowledges the hospitality offered by the Departament de Fisica of the Universitat de les Illes Balears (Spain) during the preparation of this paper. This work has been partially supported by the Programa de Cooperación Científica con Iberoamérica.

REFERENCES

Aikawa, Y., Umebayashi, T., Nakano, T., & Miyama, S. M. 1997, ApJ, 486, L51
Anglada, G. 1996, in ASP Conf. Ser. 93, Radio Emission from the Stars and the Sun, ed. A. R. Taylor & J. M. Paredes (San Francisco: ASP), 3
Bally, J., & Lane, A. P. 1991, in ASP Conf. Ser. 14, Astrophysics with Infrared Arrays, ed. R. Elston (San Francisco: ASP), 273
Corcoran, D., Ray, T. P., & Mundt, R. 1993, A&A, 279, 206
Doyon, R., & Nadeau, D. 1988, ApJ, 334, 883
Garay, G., Ramírez, S., Rodríguez, L. F., Curiel, S., & Torrelles, J. M. 1996, ApJ, 459, 193
Gómez, J. F., & D'Alessio, P. 1995, Rev. Mexicana Astron. Astrofis. Serie de Conf., 1, 339
Hartigan, P., Carpenter, J. M., Dougados, C., & Skrutskie, M. 1996, AJ, 111, 1278
Hayashi, S. S., Hasegawa, T., & Kaifu, N. 1988, ApJ, 332, 354
Ho, P. T. P., Moran, J. M., & Rodríguez, L. F. 1982, ApJ, 262, 619
Hughes, V. A. 1988, ApJ, 333, 788
Hughes, V. A., & Wouterloot, J. G. A. 1984, ApJ, 276, 204
Johnson, H. L. 1957, ApJ, 126, 121
Kylafis, N. D., & Norman, C. 1986, ApJ, 300, L73
Lane, A. P. 1989, in ESO Workshop on Low-Mass Star Formation and Pre–Main-Sequence Objects, ed. B. Reipurth (Garching: ESO), 331
Li, Z.-Y., & Shu, F. H. 1996, ApJ, 472, 211
Loren, R. B., Wootten, A., Sandqvist, Aa., Friberg, P., & Hjalmarson, Å. 1994, ApJ, 287, 707
Martín-Pintado, J., Bachiller, R., & Fuente, A. 1992, A&A, 254, 315
Morfill, G. E., Tscharnuter, W., & Völk, H. J. 1985, in Protostars and Planets II, ed. D. C. Black & M. S. Matthews (Tucson: Arizona Univ. Press), 493
Narayanan, G., & Walker, C. K. 1996, ApJ, 466, 844 (NW96)
Reynolds, S. P. 1986, ApJ, 304, 713
Rodríguez, L. F., Garay, G., Curiel, S., Ramírez, S., Torrelles, J. M., Gómez, Y., & Velázquez, A. 1994, ApJ, 430, 713
Rodríguez, L. F., Ho, P. T. P., & Moran, J. M. 1980, ApJ, 240, L149
Sargent, A. I. 1977, ApJ, 218, 736
———. 1979, ApJ, 233, 163
Scoville, N. Z., Carlstrom, J. E., Chandler, C. J., Phillips, J. A., Scott, S. L., Tilanus, R. P. J., & Wang, Z. 1993, PASP, 105, 1482
Shang, H., Shu, F. H., & Glassgold, A. E. 1998, ApJ, 493, L91
Shu, F. H., Najita, J., Ostriker, E. C., & Shang, H. 1995, ApJ, 455, L155
Shu, F. H., Ruden, S. P., Lada, C. J., & Lizano, S. 1991, ApJ, 370, L31
Staude, H. J., & Elsässer, H. 1993, A&A Rev., 5, 167
Strelnitskij, V. S. 1984, MNRAS, 207, 339
Torrelles, J. M., Gómez, J. F., Rodríguez, L. F., Curiel, S., Ho, P. T. P., & Garay, G. 1996, ApJ, 457, L107
Torrelles, J. M., Ho, P. T. P., Rodríguez, L. F., & Cantó, J. 1986, ApJ, 305, 721
Torrelles, J. M., Verdes-Montenegro, L., Ho, P. T. P., Rodríguez, L. F., & Cantó, J. 1993, ApJ, 410, 202
van Dishoeck, E. F., Blake, G. A., Draine, B. T., & Lunine, J. I. 1993, in Protostars and Planets III, ed. E. H. Levy & J. I. Lunine (Tucson: Arizona Univ. Press), 163
Wolfire, M. G., & Königl, A. 1993, ApJ, 415, 204